Spectral Analysis and Photofragmentation Dynamics of the Perdeuteromethoxy Radical

Brian E. Applegate, Michael B. Pushkarsky, and Terry A. Miller*

Laser Spectroscopy Facility, Department of Chemistry, The Ohio State University, 120 W. 18th Avenue, Columbus, Ohio 43210

Received: October 23, 1998; In Final Form: January 13, 1999

The $\tilde{A}^2A_1-\tilde{X}^2E$ electronic spectrum of the CD_3O radical has been investigated in detail. By using a variety of techniques, including rotational structure analysis, over 65 bands terminating on different vibronic levels of the $\tilde{A}$ state have been assigned. The branching ratios for fluorescence decay vs photofragmentation of these same levels have also been determined. The detailed spectroscopic mapping of the $\tilde{A}$ state vibronic structure is used to interpret the dynamical observations. The fragmentation is found to be rather mode specific, with ν_3, the C−O stretch, being a major promoting mode, while ν_2, the umbrella motion, is not. Unexpectedly the methyl rock, ν_6, also appears to be an effective promoting mode.

I. Introduction

The interest in perdeuteromethoxy is derived from its relationship to its undeuterated parent. Methoxy has been the subject of a great many studies, both theoretical[1−7] and experimental.[8−27] This interest is due in part to the importance of the photochemistry[28−31] of this radical to atmospheric, combustion, and other related chemical processes. Both because of its practical significance and its prototypical nature, methoxy's intramolecular dynamics have frequently been studied as a function of its energy and mode. A recent study,[20] which produced this type of data, has shown that the rate of photofragmentation in the $\tilde{A}^2A_1$ state of methoxy is highly correlated with the vibrational mode to which it is excited. Complementary experiments by Neumark[21,22] and co-workers provide additional information about the nature and energy content of the fragments produced.

The path to photofragmentation in methoxy likely lies along one (or more) of the three predicted[5−7] repulsive states, $^4A_2$, ^4E, and $^2A_2$, which cross the $\tilde{A}^2A_1$ state potential as depicted in Figure 1. All three of these repulsive states result in the fragmentation process

$$CH_3O(\tilde{A}^2A_1) \rightarrow CH_3(\tilde{X}^2A_2'') + O(^3P) \qquad (1)$$

Indeed, although other channels are energetically open, these fragmentation products have been confirmed by Neumark and co-workers[21,22] to be the only significant ones at the energies investigated in our work. In CH_3O, fragmentation from these repulsive states has been shown[20] to start at six quanta of the Fermi multiplet, $(\nu_2 + \nu_3)^6$, and continues to be mode selective well above this threshold. Unfortunately, the Fermi resonance between ν_2 and ν_3 in the spectrum of methoxy makes it impossible to clearly determine the contributions of the individual modes, ν_2 and ν_3, to this photodissociative process. Both modes could logically promote photofragmentation via the above path. Obviously, ν_3, the C−O stretch would be important for breaking the C−O bond, but so could be the umbrella mode, ν_2, as it moves the methyl group toward the planar geometry required by the resulting methyl fragment.

In this paper, we report the photofragmentation dynamics of the CD_3O radical, where the Fermi resonance between ν_2 and ν_3 is removed. We use a set of techniques including laser-induced fluorescence (LIF), fluorescence temporal decay (FTD), and a novel technique of fluorescence depletion spectroscopy (FDS) to provide unambiguous vibronic assignment of the $\tilde{A}^2A_1$ electronic state of CD_3O and using these assignments proceed to characterize photofragmentation of the radical as a function of total energy content and the particular vibrational mode into which the energy is deposited.

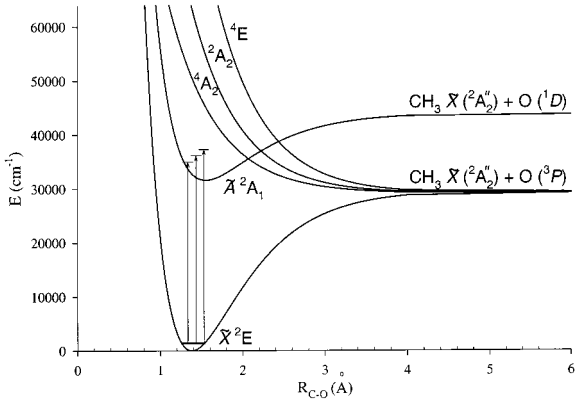

Figure 1. Cut through the potential energy surfaces of methoxy along the C−O bond (R_{C-O}). Laser excitation from the vibrationless level of the $\tilde{X}$ state to various levels of the $\tilde{A}$ state is indicated.

Having collected an extensive database for methoxy and its deuterated derivative, we relate these results to the molecular dynamics of the $\tilde{A}^2A_1$ state. In particular, we demonstrate how the observed energy-dependent and mode-specific fragmentation can be explained in terms of a "transition state" with a threshold in the C−O bond length at which crossing between the $\tilde{A}^2A_1$ state and the repulsive state occurs, followed by fragmentation into products, an O atom plus a methyl radical. Besides strong mode selectivity in the fragmentation, we also observe some coupling between particular modes and link it to anharmonic interactions.

II. Experimental Section

A. LIF and FTD Experiments. The free jet expansion and most experimental considerations for this study have been

10.1021/jp984141n CCC: $18.00
Published on Web 02/27/1999

presented previously[11] but will be briefly summarized here. The deuterated methoxy radicals were formed by photolysis of deuterated methyl nitrite seeded in helium carrier gas by a KrF excimer laser (Lumonics Excimer-500). The expansion was formed using a commercial pulsed nozzle (General Valve, IOTA One) with a 0.75 mm orifice. In order to achieve maximum vibrational cooling of the molecules, while taking the LIF spectrum, a Teflon cooling fixture as described by Powers et al.[15] was attached to the nozzle. This fixture consisted of a Teflon disk 0.5 cm thick with a preexpansion channel 2 mm in diameter. The photolysis laser crossed the preexpansion channel in the center of the Teflon disk thereby allowing the hot radicals to partially cool prior to the final expansion. The stagnation pressure of helium used when the Teflon fixture was attached was approximately 300 psi. Although the vibrational temperature was much lower when the fixture was used, some increased congestion of the rotational spectrum indicated that the rotational temperature was slightly higher. After the vibrationally cold LIF spectrum was obtained and reliable vibronic assignments were made, the fixture was removed in order to record fluorescence temporal decays, as it considerably decreased the LIF intensity.

In LIF the fluorescence from the perdeuteromethoxy radicals was collected with an *F*/1 quartz lens and projected onto an EMI 9659B photomultiplier tube. The signal from the photomultiplier was sent to a digital 175 MHz two-channel oscilloscope (LeCroy 9400a) and then stored on a computer. All spectral frequency calibration was performed by scanning an Fe/Ne hollow cathode lamp while simultaneously collecting the LIF from perdeuteromethoxy. The error limits in the frequency measurements are derived from the accuracy of the measurement of the line's frequency and its line width. From calibration of multiple scans, the estimated absolute accuracy of our frequency values is ± 0.5 cm^{-1}.

The LIF and FTD setups were very similar. In the FTD experiment the probe laser was tuned to a particular rotational line of a given vibronic band and the time-resolved fluorescence decay was recorded. The temporal resolution was determined by the PMT and associated electronics and is estimated as 20 ns. For most vibronic bands the fluorescence temporal decay was taken for only the strongest portion of the transition as the rotational structure of these transitions are only partially resolved. Where multiple measurements were taken of different parts of the band, no deviation of lifetime beyond experimental accuracy was observed.

When fluorescence temporal decay was recorded the focusing *F*/1 lens was removed to prevent excited molecules from leaving the viewing region over the time it takes them to emit. (The longest natural lifetime was over 2 μs, during which time molecules in a He expansion travel a few millimeters.)

B. FDS Experiment. For all setups of the FDS experiment, the Teflon fixture used in the LIF or FTD experiments was removed from the front of the nozzle. The jet was crossed downstream from the nozzle with a "probe" laser for which the frequency was adjusted to pump a particular rotational level of a low-lying vibronic level of the $\tilde{A}$ state. The fluorescence resulting from this laser was monitored. A second "depletion" laser was set counterpropagating along the probe laser direction and its frequency scanned over the region of interest. When the depletion laser frequency is scanned over a transition terminating on a photofragmenting level of the molecule and originating from the same rovibronic level as the transition excited by the probe laser, the fluorescence from the probe laser decreases due to loss of population of the lower level by excitation and subsequent dissociation.

An improved signal to noise ratio was achieved in the FDS experiments by splitting the probe beam and sending it through the expansion at two symmetrical locations and only overlapping one of the beams with the depletion beam. If the fluorescence from each of the two probe beams is detected separately, the beam which is not overlapped with the depletion beam can be used as a reference to normalize shot-to-shot fluctuations in the fluorescence resulting from variations in the photolysis and probe lasers as well as the jet expansion. To monitor separately LIF signals from two regions of the expansion, a special setup is required. Two arrangements of this type, using either an intensified CCD detector or two PMTs with a razor blade inserted into the jet, have been described previously in our recent studies[20,32] of the CH_3O and CF_3S radicals. Although the use of the CCD is a big improvement compared to a single beam technique, the detector software is slower and the detector is noisier and less sensitive than a PMT. On the other hand, the presence of a razor blade in the vicinity of the probed regions of the jet is a strong source of scattered light.

To improve on this technique, we once again have modified our detection system. To enable the use of two PMTs without the blade, as illustrated in Figure 2, we used two lenses to focus the light sources from the two sides of the expansion onto the plane where a quartz prism was placed such that its lower edge was located between the two images. This arrangement allows the lower image to be propagated forward and reach PMT1 while the upper image was directed to PMT2. In this arrangement the first collimating lens was *F*/1, $d = 2$ in. while the second one *F*/1.5, $d = 2$ in., allowing the distance between images in the focal plane to be 1.5 times larger than the separation between the probe and reference beams. An optical quality 1 in. prism was mounted on adjustable mounts which were used to optimize discrimination between the two images. UV 34 filters for the PMT's were used to discriminate against scattered light from the photolysis and probe/depletion lasers.

The probe laser (HyperDye 300 Lumonics Dye Laser) was pumped by an Excimer laser (Lambda) and after frequency doubling produced up to 0.5 mJ/pulse of UV power at a resolution of 0.2 cm^{-1}. Over the course of the FDS experiments the probe laser was tuned to the strongest rotational line in the 3_0^4 band. The laser was split into separate probe and reference beams by a thick (8mm) quartz window placed at a steep angle.

The depletion laser was originally a MOPO/FDO pumped by a GCR Nd:YAG on loan from Spectra Physics. The MOPO produced up to 80 mJ/pulse of emission at the fundamental frequency while the built-in frequency doubler (FDO) produced up to 7 mJ/pulse of UV. Unfortunately the MOPO/FDO had a gap of 0.1 nm between frequency regions where two different BBO crystals produced the doubled output.

A PDL 2 Lumonics Dye Laser pumped by DCR 2 Nd:YAG laser was used in the region of the gap around 280 nm. The PDL2/DCR output frequency doubled by an Inrad doubler provided up to 1 mJ/pulse of UV power.

The delay between depletion and probe lasers was set at 50−100 ns. The two LIF time-resolved waveforms from PMT1 and PMT2 were recorded by two channels of a Lecroy digital scope and transferred to a PC through a GPIB interface using LabView 4.0 software. The ratio of the two integrated areas of the fluorescence temporal decays plotted vs the frequency of the depletion laser constitutes the FDS spectrum.

C. Synthesis of Precursor. The synthesis of the methyl-*d* nitrite, as described previously[11] for methyl nitrite, was made by dropwise addition of dilute, deuterated sulfuric acid to a solution of sodium nitrite and methyl-*d* alcohol. The gaseous

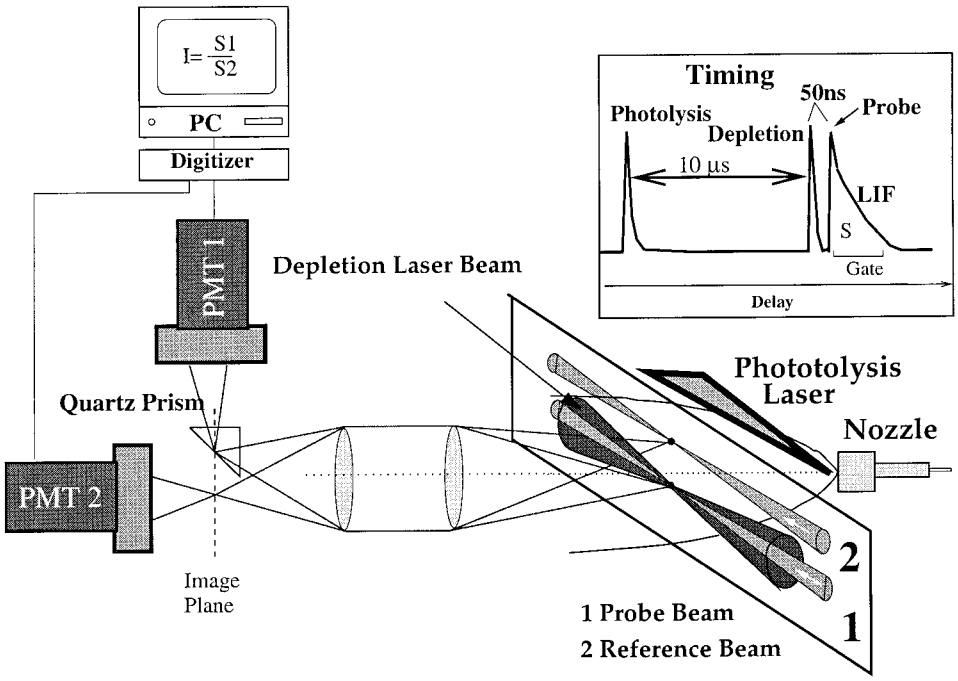

Figure 2. Experimental arrangement of the fluorescence depletion spectroscopy (FDS) apparatus.

product was then collected and used with its vapor pressure being controlled by a dry ice−isopropyl alcohol bath.

III. Vibrational Assignments of the $\tilde{A}^2A_1$ State

The spectrum of perdeuteromethoxy was previously recorded and assigned by Foster et al.[11] However, recent developments have suggested that there may be some limitations with those assignments especially with the higher energy transitions, precisely where we expect to observe the greatest amount of dynamics taking place. The recent reassignment of the methoxy spectrum[20] along with our greater ability to vibrationally and rotationally cool the molecule leaves us in a better position to assign the complete perdeuteromethoxy spectrum. To a large extent the assignments of Foster et al.[11] are correct and in those cases we will only note that our assignments do agree and refer the reader to the work of Foster et al.[11] for supporting arguments.

The LIF spectrum in Figure 3 shows a very rich and fairly complicated spectrum for perdeuteromethoxy. A summary of all our experimental observations is in Table 1. The first column gives the method by which the feature was observed. The second column gives the assignment of the feature. The third column in this table gives the frequency in cm^{-1} relative to the vibrationless level of the $\tilde{A}^2A_1$ state. The last column gives the lifetime of the feature, which will be discussed in detail in section IV.

A few words of explanation on the procedure for determining the values of the frequencies are in order. In the present work we were able to resolve the rotational structure for most of the bands and extensively used the argument[20] of similarity of rotational contours (see Figure 4) for assignment of modes of the same symmetry in the fluorescence spectrum. However, we did not perform simulations of rotational structure on most of the bands primarily because the most important information extractable from the laborious analysis has already been deduced from our previous work on the LIF of CH_3O. The major shortcoming of this lack of rotational analysis is that in the present paper we did not obtain the band origin as a parameter from the complete rotational analysis. We therefore quote frequencies as the centers of the bands in the LIF spectrum.

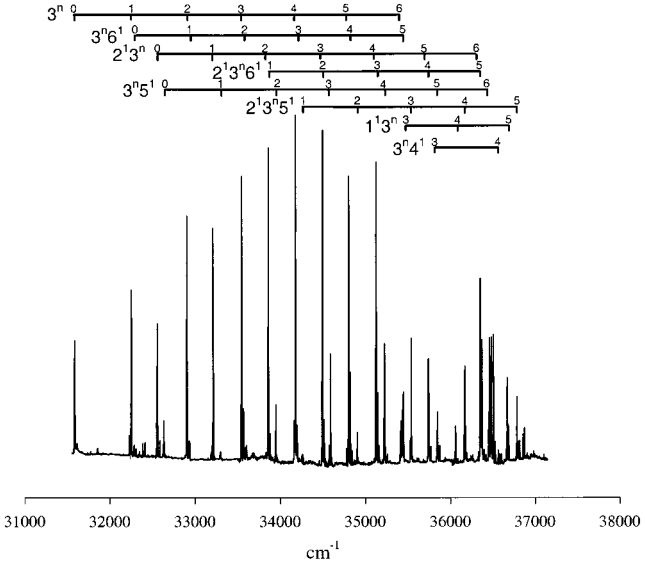

Figure 3. LIF spectrum of perdeuteromethoxy with vibrational assignments as indicated.

The error between the two measurements should not be more than a few cm^{-1}.

Using the improved spectrum, due to the increased cooling achieved with the use of the Teflon fixture, vibrational assignments of most of the features in the LIF spectra were achieved unambiguously by predicting approximate positions by extending nearly harmonic progressions and then confirmed by identifying rotational profiles.[20] With the elimination of the congestion due to hot features, the fundamentals of the lower frequency modes can readily be identified and assigned, as given in Table 1. Existence of an assigned spectrum for protonated methoxy[19] helped significantly with the assignment of the LIF spectrum of CD_3O. CH_3O and CD_3O spectra are very similar except for the absence of Fermi resonance between $2\nu_3$ and ν_2 for CD_3O.

The frequency of the lower spin component of the $\tilde{A}^2A_1-\tilde{X}^2E$ 0_0^0 transition has been determined independently by this

TABLE 1: Observation Techniques, Assignments, Relative Frequencies, and Lifetimes of the $\tilde{A}^2A_1$ Vibrational States

obsd[a]	assignment[b]	freq[c] (cm^{-1})	lifetime[d] (ns)
L	0^0	0	2800
L	3^1	664	2690
L	6^1	697	
L	2^1	970	2780
L	5^1	1047	2640
L	3^2	1319	2820
L	3^16^1	1345	2250
L	2^13^1	1628	2660
L	3^15^1	1711	2710
L	3^3	1962	2880
L	3^26^1	1985	2400
L	3^16^2	2018	
L	2^13^2	2275	2750
L	$2^13^16^1$	2297	
L	3^25^1	2364	2500
L	3^4	2595	2860
L	3^36^1	2613	2590
L	3^26^2	2644	
L	$2^13^15^1$	2672	3010
L	2^13^3	2912	2800
L	$2^13^26^1$	2930	2500
L	$2^13^16^2$	2959	
L	3^35^1	3006	2590
L	3^5	3220	2820
L	3^46^1	3235	2770
L	3^36^2	3258	
L	$2^13^25^1$	3319	1950
L	2^13^4	3540	3030
L	$2^13^36^1$	3557	2460
L	$2^13^26^2$	3577	
L	3^45^1	3638	2800
L	3^6	3829	502
L	3^56^1	3844	737
L	1^13^3	3851	1410
L	$2^13^35^1$	3956	2680
L	2^13^5	4157	2570
L	$2^13^46^1$	4170	2150
L	$2^13^36^2$	4183	
L	3^55^1	4260	2360
L	3^34^1	4287	2350
D	3^7	4435	*e*
L	1^13^4	4473	687
L	$2^13^45^1$	4582	
L, D	2^13^6	4764	174
L	$2^13^56^1$	4775	271
L	$1^12^13^3$	4786	
L	3^65^1	4869	309
L	$1^13^35^1$	4893	893
L	$3^55^16^1$	4921	122
L	3^44^1	4941	
D	3^8	5010	*e*
D	3^76^1	5032	*e*
L	1^13^5	5086	154
L	2^23^5	5102	1130
L	$2^13^55^1$	5198	1330
L	$2^13^34^1$	5217	1900
L	3^55^2	5230	1990
D	$3^34^15^1$(?)	5350	*e*
D	2^13^7	5363	*e*
D	$2^13^66^1$	5375	*e*
L	$1^12^13^4$	5398	
D	3^75^1	5470	*e*
L	$1^13^45^1$	5514	
D	3^54^1	5550	*e*
D	3^9	5593	*e*
D	3^86^1	5620	*e*

[a] Technique of observation, L = LIF and D = FDS. [b] All transitions originate from the vibrationless level of the $^2E_{3/2}$ spin component of the ground state. [c] Frequency relative to vibrationless level of $\tilde{A}$ state. To obtain the absolute frequency relative to the origin of the $\tilde{X}^2E$ state or the $\tilde{X}^2E_{3/2}$ spin component, add, respectively, 31 557 or 31 584 cm^{-1}. [d] Blank entries in this column indicate that the transition was too weak to obtain reliable lifetime information. [e] Lifetime $\tau_{v'}$ determined to lie between the limits 20 ns $\geq \tau_{v'} \geq$ 20 ps.

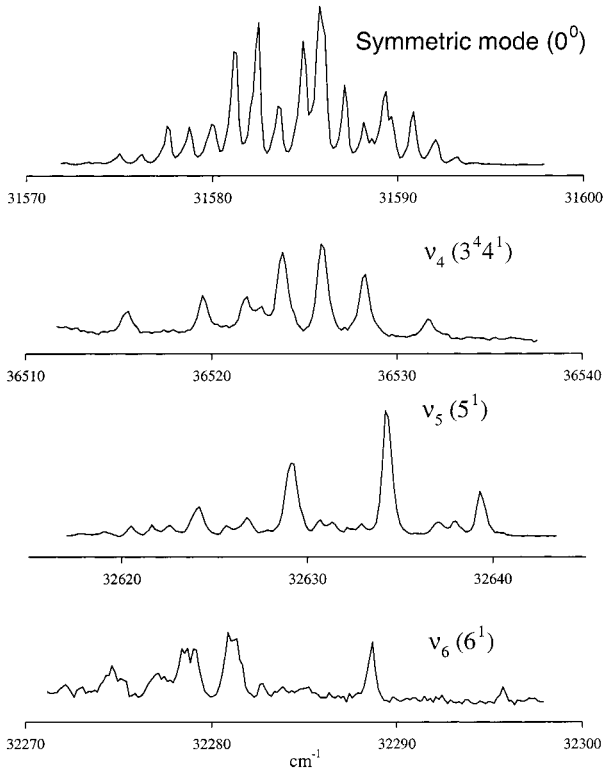

Figure 4. Rotational profiles for several vibrational modes of perdeuteromethoxy.

work to be 31 584 cm^{-1} which agrees nearly within experimental error with the value determined in the work of Foster et al.[11] of 31 581 cm^{-1}. The small discrepancy between our value for the vibrationless level and that obtained by Foster et al.[11] can further be accounted for by the difference in determining band frequencies and the rotational temperature. The method for determining the absolute band frequency in this work was as described above; however, Foster et al.[11] used the most intense portion of the band to determine the absolute frequency. Upon inspection of the rotational profile of the origin band in Figure 4 we see that the most intense portion of this band is near the center of the band. However, if the rotational temperature is raised the most intense portion of the band can easily move to the red a few cm^{-1}, resulting in an absolute frequency for the origin of 31 581 cm^{-1} using the method of Foster et al.[11]

A. Symmetric Mode Assignments. A long progression in ν_3 dominates the spectrum of perdeuteromethoxy. This is a result of the lengthening of the C−O bond upon excitation from the $\tilde{X}^2E$ to the $\tilde{A}^2A_1$ state. The first band in this progression and the first band observed after the origin is assigned as one quantum of ν_3, the C−O stretch, and has a frequency of about 667 cm^{-1}. The observed frequency is consistent with the work of Foster et al.[11] We observe this progression in ν_3 from 0 to 6 quanta in LIF and 7 to 9 quanta in FDS.

A feature at 970 cm^{-1} with similar rotational structure was assigned as ν_2 as did Foster et al. Ab initio calculations predict it to be at 984 cm^{-1}. The geometry of the methyl group does not change significantly in the electronic transition, and hence ν_2 corresponding to the symmetric C−D bend is expected to have Franck−Condon factors favoring diagonal transitions. In agreement with this idea, only transitions to one quantum of ν_2 and one or two quanta of ν_2 in combinations with ν_3 have been observed in the LIF spectrum. One should note that in CH_3O most of the activity in ν_2 was due to its strong mixing with ν_3 by Fermi resonance.

The progression in $2^1 3^n$ has been observed in fluorescence from $n = 0-6$ and in depletion for $n = 7$. One additional feature involving only ν_2 and ν_3 is a band at 5102 cm^{-1} assigned as $2^2 3^5$ and seen only in LIF. These assignments are based on the frequencies of the bands and the fact that their rotational contours are consistent with a totally symmetric vibration.

The third symmetric mode ν_1, the symmetric C−D stretch, was observed only in combinations with ν_2 and ν_3. Foster et al. assigned a long progression in $1^1 3^n$ ($n = 1-5$) yielding a frequency for ν_1 of 2015 cm^{-1}. We believe that this assignment is incorrect (see below for details) because these bands do not have the rotational structure of a totally symmetric transition. Instead, two other progressions containing ν_1 are assigned in this spectrum. The first progression begins with a feature at 3851 cm^{-1} which has been assigned as $1^1 3^3$. This feature has not been previously observed. The basis for this assignment lies in its rotational profile and relative frequency. The rotational profile of this band is very similar to that of the other totally symmetric bands. Its relative frequency is consistent with the ab initio calculations. In addition, there are no other possible symmetric combinations unaccounted for in this region. This progression has the general form $1^1 3^n$ where $n = 3-5$ have been observed. The other progression thought to contain ν_1 starts with a feature at 4786 cm^{-1} which is assigned as $1^1 2^1 3^3$. The basis for this assignment is the same as that for the $1^1 3^n$ progression, the rotational profile and relative frequency make it the most probable choice. This progression has the general form $1^1 2^1 3^n$ where $n = 3-5$ have been observed.

B. Asymmetric Modes. The band at 697 cm^{-1} has been assigned to the lowest frequency e vibrational mode ν_6 (rocking motion). Nominally, this band, along with the other e modes, is observed because the vibrationless level of the $\tilde{X}$ state contains some e character due to the Jahn−Teller effect. The frequency of ν_6 was not reported previously probably due to its low intensity and its close proximity to ν_3, which could easily result in it appearing at most as a small shoulder on ν_3, in a rotationally warmer spectrum. The experimental result is in satisfactory agreement with the ab initio value.

The rotational structure of ν_6 is very distinct and was used to help identify combination bands involving ν_6. Two progressions have been so identified and assigned to $3^n 6^1$ and $2^1 3^m 6^1$ where $n = 1-5$, $m = 1-5$ have been observed in fluorescence and $n = 7-8$, $m = 6$ have been observed in depletion. $3^6 6^1$ was not observed and is likely too weak to be seen by either method.

Our assignment of the fundamental of ν_5 at 1052 cm^{-1} is consistent with the assignment of Foster et al. and the ab initio calculations. Once again, this vibration has a very distinctive rotational signature which can be used to confirm the assignment. The mode ν_5 is seen to exist in two long progressions of combinations with the ν_3 and ν_2. The general forms for these progressions are $2^1 3^n 5^1$ and $3^m 5^1$ where $n = 1-5$, $m = 1-6$ have been observed in fluorescence and $n = 6$ has been observed in depletion. These features again have the distinctive rotational signatures of ν_5 and can easily be identified by this structure.

The fundamental of the asymmetric C−D stretch, ν_4, has not been observed in this work but combinations of this band with ν_3 have. Foster et al. did not assign any transition involving ν_4. The assignment of $3^3 4^1$ band (4290 cm^{-1}) is based on a rotational structure different from those of ν_6, ν_5, and ν_3 and the ab initio prediction of $\omega_4 = 2266$ cm^{-1}, placing the combination close to its observed frequency. Progressions of $3^n 4^1$ and $2^1 3^m 4^1$ were observed from $n = 3-4$ and $m = 3$ in fluorescence and $n = 5$ has been observed in depletion. However, not all bands from these progressions have identical rotational structure.

There are several features in the LIF spectrum at high frequencies which have been assigned to vibrations involving two quanta of degenerate modes in combinations with ν_3. As one can learn from the analysis of the LIF of CH_3O, such a band again has a unique rotational structure. In the present work we did not simulate rotational profiles, but make this assignment on the basis of frequency, uniqueness of the appearance of the rotational profile and relative intensity (which is expected to be low for such modes). For this same reason we could not separately determine the frequency of the a and e subbands of such combinations and overtones of e modes.

Another general reason for limitations in the assignment of the bands at high frequency is that the structure of these bands does not match precisely that expected for bands terminating in vibronic levels of the types previously considered. We suspect many of the high-frequency vibronic bands have rotational structure differing from the usual patterns because of Coriolis perturbations *between* different vibronic levels. If strong enough, such perturbations could give rise to virtually unique structure for each level, the analysis of which being a nearly impossible task based upon the present data.

C. Comparison with Previous Spectral Assignments. In general, the vibrational frequencies obtained in Foster et al. and that of this work agree rather well. In the former case, values for four (ν_1, ν_2, ν_3, and ν_5) of the possible six vibrational frequencies were reported. In the present work we confirm, within reasonable experimental error, all except one (ν_1) of them, while adding values for the two remaining vibrations (ν_4 and ν_6). However, there are some discrepancies between the assignments of particular levels by Foster et al.[11] and the present work, especially in the higher frequency region of the spectrum. The inconsistencies start with the feature at 2672 cm^{-1} which we assign as $2^1 3^1 5^1$ because of its clear resemblance to the fundamental of ν_5 and the fact that we see a progression separated by 647 cm^{-1}, the frequency of the C−O stretch, ν_3. This was previously assigned[11] as $1^1 3^1$, a totally symmetric mode. This misassignment is carried on through the progression of $2^1 3^5 5^1$. The most probable reason for this discrepancy is that the spectrum of Foster et al.[11] was rotationally much hotter than the one presently recorded, resulting in less distinctive rotational profiles for the features observed.

The progression presently assigned as $1^1 3^n$ where $n = 3-5$ was previously assigned as higher overtones of ν_3, 3^n where $n = 6-8$. What was previously assigned as 3^6 is actually a clump of three bands, 3^6, $3^5 6^1$, and $1^1 3^3$. The lowest frequency band in this cluster is fairly weak. It is presently assigned as 3^6 because of its position in relation to $3^5 6^1$ which is the more easily identified combination band because of its characteristic rotational profile resembling the ν_6 fundamental. The highest frequency band of this clump is assigned as $1^1 3^3$ because of its relative frequency and rotational profile. The bands in the LIF spectrum previously assigned as 3^7 and 3^8 have been reassigned as the next bands in this progression, $1^1 3^4$ and $1^1 3^5$, respectively.

If we take a lesson from previous work[20] on CH_3O we see that the progression in the LIF spectrum for the Fermi multiplet $(\nu_2 + \nu_3)$ stops after $(\nu_2 + \nu_3)^6$ due to photofragmentation. We would expect the same sort of behavior in its deuterated derivative, and indeed we do observe the photofragmentation onsetting at the presently assigned 3^6, as is evidenced by the observation in FDS of the bands, 3^6-3^9. An additional piece of evidence is the low intensity of 3^6 relative to the other bands in the progression, which is caused by a significant depopulation

of this Ã state vibrational level by photofragmentation, consistent with its much shorter lifetime.

The final point of inconsistency arises with the features at 4869 and 4893 cm^{-1}, now assigned as $3^6 5^1$ and $1^1 3^3 5^1$, respectively. The feature at 4869 cm^{-1} was previously not observed, and the feature at 4893 cm^{-1} was assigned previously as $3^6 5^1$. Both bands exhibit the rotational profile of ν_5. Upon close inspection of the relative frequencies and intensities of the bands, one must conclude that we have now correctly assigned the band at 4869 cm^{-1} as $3^6 5^1$. If the band at 4893 cm^{-1} were to be considered a part of the $3^n 5^1$ progression, the relative spacings of the bands and the intensity would suddenly increase at $3^6 5^1$.

IV. Dynamics of the $\tilde{A}^2A_1$ State

With our extensive Ã state vibrational assignments we now have the prerequisite for a proper analysis of the excited state dynamics. Without these complete assignments the analysis of the dynamics data would be extremely difficult if not impossible. We monitor the dynamics by measuring the temporal decay of those levels that fluoresce, as well as observing the FDS of those that do not and bracketing the lifetimes of the latter, based upon the observed linewidths and other considerations.

A. Temporal Decays. For nearly all of the observed LIF features the time-resolved fluorescence was recorded. Since we were only able to partially rotationally resolve the vibrational bands we did not attempt to record temporal decays for individual rotational lines. In most cases the temporal decay was recorded for only the strongest portion of the vibronic band. The natural lifetimes obtained from these experiments are summarized in Table 1, column four. The missing lifetimes in column four indicate that for FTD, the intensity of the transition was sufficiently small so that when we removed the collection optics the signal was indistinguishable from the noise.

Generally speaking, for levels studied by FTD, there is about a 5% or 50 ns uncertainty, whichever is greater, associated with the reported values of the natural lifetime, τ_ν, where ν denotes the set of vibrational quantum numbers that label the level. For those levels observed by FDS, only a range for the lifetime can be determined. The upper limit (20 ns) is based upon the assumption that in most cases an effective quantum yield of greater than about 1% would have allowed the level's fluorescence to be observed and its FTD measured. On the other hand, lack of any line broadening for the levels presently observed by FDS indicates that their lifetimes are in excess of about 20 ps.

There is a large amount of information that can be gleaned from Table 1 about the nature of the $\tilde{A}^2A_1$ state and its dynamics. The first thing to note is that τ_0 of the vibrationless level is 2800 ns. The $\tau_{\nu'}$ for some levels observed more than 5000 cm^{-1} above the vibrationless level have values similar to τ_0, although even in these levels there exists a gradual decrease in $\tau_{\nu'}$ from 2800 to about 1700−1900 ns, presumably due to a slow variation in transition moment.

However, at 3829 cm^{-1} in energy there is an abrupt decrease in $\tau_{\nu'}$ to 502 ns for the 3^6 transition. As in methoxy we interpret this abrupt change as due to the opening of the dissociation channel and establish a range for the threshold for photofragmentation with the upper limit assigned to the 3^6 transition and a lower limit to the 3^5 transition at 3220 cm^{-1}. Above this threshold, we see a large variation in $\tau_{\nu'}$ with transitions nearly isoenergetic exhibiting $\tau_{\nu'}$s differing by orders of magnitude.

B. Analysis. The mode selectivity of the photofragmentation is most apparent when we make a plot of log $(\tau_{\nu'}/\tau_0)$ vs energy.

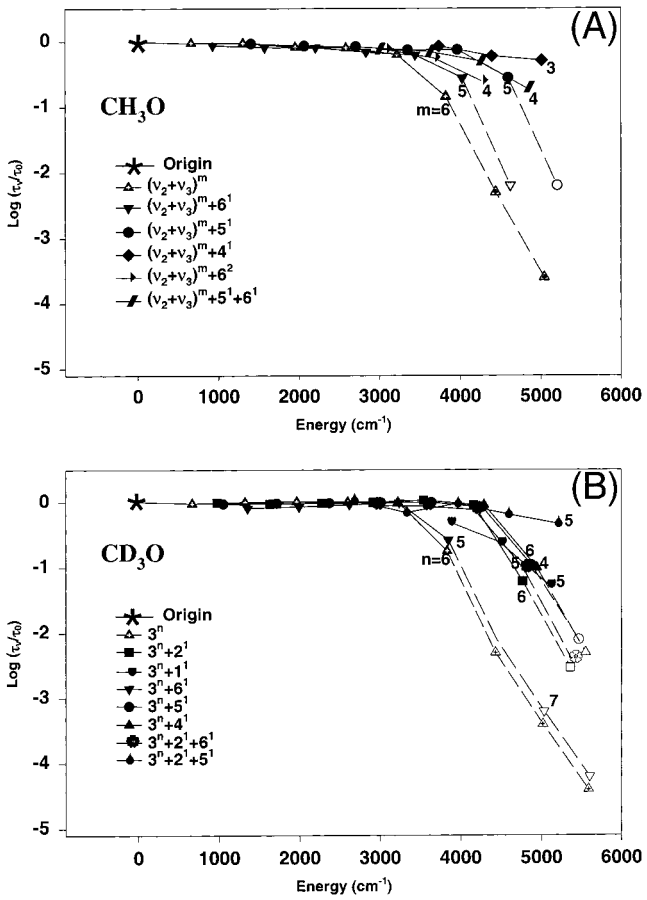

Figure 5. Plots of effective quantum yield (see text) vs energy (relative to the vibrationless level). The open symbols in the plots represent points for which the lifetimes cannot be deduced from the experimental data, but can only be determined to lie between the limits, 20 ns $< \tau_\nu <$ 20 ps. Within this range this vertical placement on the plot is arbitrary. (A) Plots of the vibrational progressions in CH_3O where m equals the number of quanta of excitation into the Fermi multiplet $(\nu_2 + \nu_3)^m$. For these plots the energy and lifetimes of the Fermi multiplets were averaged to produce the points on the plots. (B) Plots of the vibrational progressions in CD_3O where n equals the number of quanta of excitation into 3^n.

If we assume the vibrationless level decays at the radiative lifetime and therefore corresponds to a fluorescence quantum yield of 1, the ratio $\tau_{\nu'}/\tau_0$ is then the effective quantum yield of the level ν'. We show this plot in Figure 5 for methoxy and perdeuteromethoxy. Generally speaking, Figure 5 shows that there exists different sorts of fragmentation behavior depending upon which mode is excited.

If we take a closer look at Figure 5B, we can illustrate the trends involved. From this figure we can clearly see the energetic and mode dependence of the photofragmentation. From the progression in ν_3 we can see a clear threshold for photofragmentation arising between 3^5 and 3^6. For modes with excitation in 3^n with $n \leq 5$ the probability of photodissociation is nearly zero, roughly independent of energy, while for modes with excitation into 3^n with $n \geq 6$ we see a dramatic increase in the probability of photodissociation with 3^7 and higher exhibiting greater than 99% fragmentation. Roughly independent of energy, all other progressions in Figure 5B exhibit the same threshold for fragmentation for excitation in ν_3 with the exception of the combination band $3^n 6^1$. The $3^n 6^1$ bands exhibit a threshold at $4 < n < 5$. It appears that, like ν_3, ν_6 also has significant propensity for inducing photofragmentation.

If we compare these results to the mode selective photofrag-

TABLE 2: Observed Frequencies, $\omega_{e,i}$, and the Corresponding ab Initio Calculated Frequencies (cm^{-1}) and C−O Bond Extensions, X_{ν_i}, for the $\tilde{A}^2A_1$ State

	experimental (cm^{-1})			calculated			experimental (cm^{-1})			calculated	
CH_3O	ω_0	$\omega_{e,i}$	$\omega_e x_{e,i}$	$\omega_{e,i}$	X_{ν_i} (Å)	CD_3O	ω_0	$\omega_{e,i}$	$\omega_e x_{e,i}$	$\omega_{e,i}$	X_{ν_i} (Å)
ν_1	2947.8	*a*	*a*	2901	0.003	ν_1	1889[b]	*a*	*a*	2062	0.005
ν_2	1289.3[c]	1313.2(7)	7.37(25)	1320	0.007	ν_2	970	966(3)	0(2)	984	0.015
ν_3	662.4	677.2(4)	4.64(8)	636	0.082	ν_3	667	671(0.5)	5.54(7)	629	0.081
ν_4	3077.8[d]	*a*	*a*	3038	*e*	ν_4	2325[f]	*a*	*a*	2266	*e*
ν_5	1403.0	*a*	*a*	1410	*e*	ν_5	1052	*a*	*a*	1035	*e*
ν_6	929.5	951.0[g]	7.1[g]	977	*e*	ν_6	697	698(4)	5.12(1.64)	726	*e*

[a] Insufficient data was obtained to determine the ω_e and $\omega_e x_e$ of these modes. [b] Established by subtracting the relative frequency of 3^3 from $1^1 3^3$. [c] Perturbed by Fermi resonance with 3_0^2. [d] Established by subtracting the relative frequency of 3^1 from $3^1 4^1$. [e] There is zero C−O bond extension for any asymmetric mode. [f] Established by subtracting the relative frequency of 3^3 from $3^3 4^1$. [g] Based upon 6^1 frequency and average frequency of a and e components of 6^2.

mentation in methoxy we see a very similar behavior with the threshold for photofragmentation occurring between $m = 5$ and 6 in the Fermi multiplet, $(\nu_2 + \nu_3)^m$, for nearly all progressions in the spectrum. At this point we are able to answer the question posed in the Introduction as to which mode is primarily responsible for producing photofragmentation in methoxy, ν_2 or ν_3 or both? The perdeuteromethoxy data clearly shows us that ν_3, the C−O stretch, is the mode responsible for producing photofragmentation. The combination bands $2^1 3^n$ and $2^1 3^n 5^1$ both exhibit the same threshold for photofragmentation in ν_3 quanta as the pure 3^n progression. Therefore, the excitation in ν_2 has no direct bearing on the photodissociation process. It appears that the reaction pathway to fragmentation lies along the C−O stretching mode and only after the bond is broken does the CH_3 fragment attempt to assume its equilibrium planar geometry.

It is worthwhile to discuss our present results for CH_3O and CD_3O and those presented recently by Osborn et al.[22] Our experiments are quite complementary. Basically, as a function of photon energy we detect disappearance of the parent methoxy radical while they detect the appearance of fragments. Our experiments, primarily due to jet cooling, are of much higher resolution (a few tenths of cm^{-1} compared to about 50 cm^{-1}) and hence provide a much clearer picture of the mode selectivity in the dissociation. However, our experiments provide no details about the fragments, while those of Osborn et al. provide considerable characterization of the nature of the fragments and their translational energy.

For methoxy, both sets of experiments agree that ν_3, nominally the C−O stretch, is a prime promoting mode for photofragmentation with a threshold at $(\nu_2 + \nu_3)^6$, while energy deposited in ν_2, nominally the umbrella motion, is relatively ineffective in CD_3O, the only isotopomer where the ν_2 motion can be uniquely resolved. The results of Osborne et al., showing considerable energy in the umbrella motion of the methyl fragment, are completely consistent with this conclusion. Our results further show that energy deposited in ν_5, ν_4, or ν_1 (CD_3O) is similarly ineffective.

Surprisingly, however, our present results show that energy deposited in ν_6, the asymmetric rock, is nearly as effective in CD_3O as placing the energy in ν_3. For CH_3O, ν_6 is also effective in promoting fragmentation, although whether it is as efficient as ν_3 is hard to determine from our data. Osborn et al. also discussed the promoting efficiency of ν_6. They conclude that "in CH_3O the combination band $3^n{}_0 6^1{}_0$ dissociates for $n = 5$, while in CD_3O combination band dissociation is not observed unless $n \geq 6$." For CH_3O our observations are in agreement. However, for CD_3O the situation is more complex. Our greater resolution and rotational cooling allow us to observe the nearly isoenergetic levels 3^6 and $3^5 6^1$ independently, and we see that they both have essentially the same photofragmentation rates. Separated by only 15 cm^{-1}, 3^6 and 3^5 6^1 are unresolved in the experiments of Osborn et al., leading to their conclusion.

While we believe that in both CH_3O and CD_3O, energy deposited in ν_6 is effective in promoting photofragmentation, it is not particularly clear why this should be so. Perhaps slightly decreasing the OCH angle leads to a lower energy "pass" over the transition state barrier.

C. Discussion. While ν_3 carries the bulk of the C−O extension, the other symmetric, normal modes have some C−O stretch involvement. It is therefore interesting to consider directly the fragmentation dependence upon C−O bond extension, independent of normal mode.

In order to account for the mixing of the internal coordinates in the normal modes, it is necessary to calculate the actual C−O bond extensions in the various vibrational levels. To this end, we performed an ab initio calculation on methoxy, optimizing the geometry at the RHF/6-31g* level. Then an analytical frequency calculation was performed. The resulting Cartesian coordinates for each mode were converted to internal coordinates and the classical turning point computed. The deviations, X_{ν_i}, between the equilibrium C−O bond length and the outer classical turning points for $\upsilon_i = 0$ are given in Table 2 for each symmetric mode, ν_i. No bond extensions are shown for the asymmetric modes because they are computationally virtually zero as would be expected given the nominal C_{3v} symmetry of the molecules.

At the outer turning point of any vibrational level, the kinetic energy must be zero, so for a classical harmonic oscillator, we have

$$^1/_2 k X_\upsilon{}^2 = h\omega(\upsilon + {}^1/_2) = k X_{\nu_i}{}^2(\upsilon + {}^1/_2) \qquad (2)$$

where X_υ is the classical turning point for the υth level. To compute the maximum C−O bond extension, ΔR_{CO}, for a given vibrational level we write

$$\Delta R_{CO} = (2\upsilon_1 + 1)X_{\nu_1} + (2\upsilon_2 + 1)X_{\nu_2} + (2\upsilon_3 + 1)X_{\nu_3} \qquad (3)$$

Ignoring the effects of anharmonicities on the bond extension, i.e., assuming a harmonic oscillator potential, dictates that these calculated bond extensions should be considered as lower limits to the true bond extension.

We believe the photofragmentation process can be viewed as analogous to walking toward a cliff. Once you have stepped over, the process is essentially irreversible. Similarly, when a molecule reaches the threshold for the C−O bond extension threshold it has a high probability of fragmenting. In our analysis we therefore use the maximum bond extension when all three vibrations are in phase, even though the molecule will only

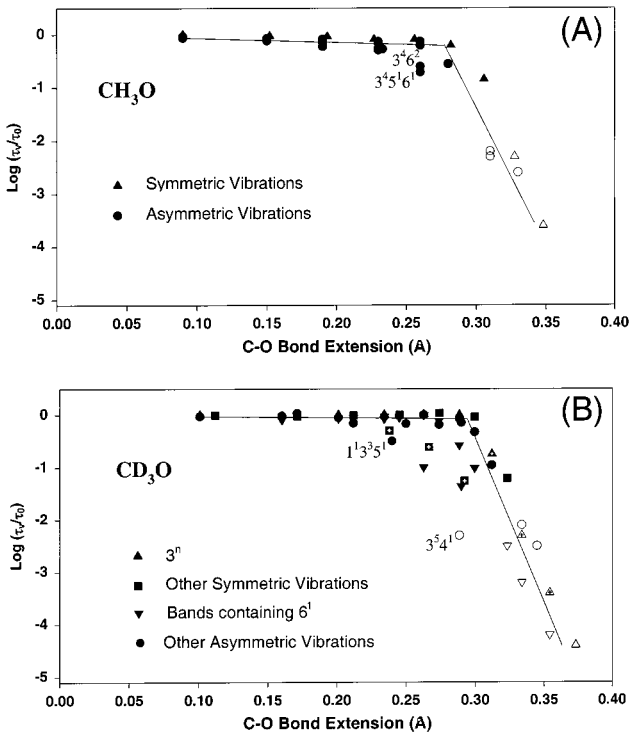

Figure 6. Plots of effective quantum yield (see text) vs energy (relative to the vibrationless level) for selected modes. The open symbols in the plots represent points for which the lifetimes cannot be precisely deduced from the experimental data, but can only be determined to lie between the limits, 20 ns $< \tau_v <$ 20 ps. Within this range this vertical placement on the plot is arbitrary. The *n* values on the plot denote the number of quanta of excitation into 3^n.

spend a relatively small amount of time sampling this portion of the potential.

An explanation is also necessary for how the bond extension was calculated for levels involving the Fermi resonance between ν_2 and ν_3 in CH_3O. Here we again argue that the maximum bond extension should be used in the analysis. To that end we have considered each Fermi multiplet as if it were pure ν_3, since ν_3 has the maximum C−O bond extension and all features in the multiplet will visit this part of the potential a portion of the time. (For Figures 5 and 6 the experimental lifetime for the features of each Fermi multiplet were averaged before calculating the quantum yield.)

Figure 6, using the calculated C−O bond extensions for each observed level, shows a simpler picture of the photodissociation dynamics than that depicted in Figure 5. We have essentially replaced two variables, energy and number of quanta of excitation in ν_3, by one, C−O bond extension. If we start with the parent molecule, methoxy, we see in Figure 6A a very nice correlation between the amount of C−O bond extension and the rate of fragmentation. We can clearly see a threshold for photofragmentation at ≈0.28 Å. Beyond this threshold essentially all of the molecules fall apart to products. This threshold may be compared to the C−O bond extension of 0.41 Å calculated by Morokuma et al.[7] at the lowest crossing.

Figure 6B for deuterated methoxy shows generally a very similar picture to that observed for CH_3O, with a very comparable C−O bond extension threshold for dissociation. However, we do note that in Figure 6B there are a few outlying points for which an explanation is in order. There are six data points which contain crosses. The three that lie substantially below the line belong to the $1^1 3^{n-3}$ progression, while the three approximately on the line belong to the 3^n progression. We believe that these terminating levels of the same symmetry undergo mixing due to nonharmonic terms in the potential. The pairs (all close energetically) which are mixed are 3^6 and $1^1 3^3$ (22 cm^{-1} separation), 3^7 and $1^1 3^4$ (38 cm^{-1} separation), and 3^8 and $1^1 3^5$ (76 cm^{-1} separation). The result is anamolously short lifetimes for the three members of the $1^1 3^n$ progression, considering only their C−O bond extension.

There are, however, other outlying points in Figure 6B for which no particular mode mixing is easily identifiable. Several of these, marked with ▽'s, contain quanta of ν_6, predominately the rocking motion, which has been already argued to be an independent promoting motion. Hence these points should be expected to fall below the line. It is also useful to note that the two points that obviously fall below the line for CH_3O in Figure 6A also contain contributions from ν_6.

An additional couple of points in Figure 6B, corresponding to levels $1^1 3^3 5^1$ and $3^5 4^1$, also appear to fall below the line. While there is no obvious mode mixing occurring here, as between the $1^1 3^{n-3}$ and 3^n progression, both levels lie at high energies such that such effects cannot be ruled out.

Generally speaking, we see a clear propensity for energy being localized in the C−O bond stretch. Methoxy then obeys a simple one-dimensional reaction path picture, going through a transition state with a critical C−O bond length, and then passes on to products. Our data indicate a few deviations from this picture, which are mostly explained in terms of local perturbations that mix modes. While such mode mixing is clearly not the dominant process in the energy region investigated, it suggests that with sufficient energy the molecule will eventually evolve to the now familiar statistical limit, within the vibrational manifold of the $\tilde{A}$ state, and possibly eventually also including the $\tilde{X}$ state.

V. Conclusions

We have assigned the LIF spectrum of perdeuteromethoxy using several techniques which have significantly improved our ability to make assignments over previous work. These advantages included better rotational cooling and rotational structure analysis. We have also obtained a vibrationally much colder spectrum. In addition to previous LIF observations we also were able to use the FDS method to help confirm assignments and to push the observations further to the blue.

With this refined spectroscopic analysis we are able to make a similar analysis of the mode selective photodissociation in CD_3O as was previously done on CH_3O and CF_3S. We have established a threshold for photofragmentation in CD_3O to exist between 5 and 6 quanta of ν_3. We have also shown in perdeuteromethoxy that the contribution to photofragmentation of the energy deposited in ν_2 is negligible, and the same is likely also true for CH_3O. On the other hand, activity in ν_6 appears to have an independent inducing effect for both isotopomers. Indeed in CD_3O energy deposited in ν_6 appears essentially as effective as that deposited in ν_3. Our analysis of the dependence of photofragmentation yield on C−O bond extension shows a clear and consistent threshold for both isotopomers.

Acknowledgment. The authors acknowledge the support of this work via NSF grant CHE 9320909. We also thank Spectra Physics for the loan of the MOPO. We thank Tim Barckholtz for performing the ab initio calculations and Mr. Zhi Yao for help in gathering preliminary experimental data.

References and Notes

(1) Yarkony, D. R.; Schaefer, I. H. F.; Rothenberg, S. *J. Am. Chem. Soc.* **1974**, *96*, 656.

(2) Ohkubo, D.; Fujita, T.; Sato, H. *J. Mol. Struct.* **1977**, *36*, 101.
(3) Bent, G. D.; Adams, G. F.; Bartram, R. H.; Purvis, G. D.; Bartlett, R. J., *J. Chem. Phys.* **1982**, *76*, 4144.
(4) Saebo, S.; Radom, L.; Schaefer, I. H. F. *J. Chem. Phys.* **1983**, *78*, 845.
(5) Jackels, C. F. *J. Chem. Phys.* **1982**, *76*, 505.
(6) Jackels, C. F. *J. Chem. Phys.* **1985**, *82*, 311.
(7) Cui, Q.; Morokuma, K. *Chem. Phys. Lett.* **1996**, *263*, 54−62.
(8) Misra, P.; Zhu, X.; Hsueh, C. Y.; Halpern, J. B. *Chem. Phys.* **1993**, *178*, 377.
(9) Misra, P.; Zhu, X. *Spectrosc. Lett.* **1993**, *26*, 389.
(10) Misra, P.; Zhu, X.; Nur, A. *Spectrosc. Lett.*, **1992**, *25*, 639.
(11) Foster, S. C.; Misra, P.; Lin, T.-Y.; Damo, C. P.; Carter, C. C.; Miller, T. A. *J. Phys. Chem.* **1988**, *92*, 5914.
(12) Liu, X.; Damo, C. P.; Lin, T. Y.; Foster, S. C.; Misra, P.; Yu, L.; Miller, T. A. *J. Phys. Chem.* **1989**, *93*, 2266.
(13) Garland, N. L.; Crosley, D. R. *J. Phys. Chem.* **1988**, *92*, 5322.
(14) Fuke, K.; Ozawa, K.; Kaya, K. *Chem. Phys. Lett.* **1986**, *126*, 119.
(15) Powers, D. E.; Hopkins, J. B.; Smalley, R. E. *J. Phys. Chem.* **1981**, *85*, 2711.
(16) Inoue, G.; Akimoto, H.; Okuda, M. *Chem. Phys. Lett.* **1979**, *63*, 213.
(17) Inoue, G.; Akimoto, H.; M. O. *J. Chem. Phys.* **1980**, *72*, 1769.
(18) Lee, Y. Y.; Wann, G. H.; Lee, Y. P. *J. Chem. Phys.* **1993**, *99*, 9465.
(19) Powers, D. E.; Pushkarsky, M.; Miller, T. A. *J. Chem. Phys.* **1997**, *106*, 6878.
(20) Powers, D. E.; Pushkarsky, M.; Miller, T. A. *J. Chem. Phys.* **1997**, *106*, 6863.
(21) Osborn, D. L.; Leahy, D. J.; Neumark, D. *Chem. Phys. Lett.* **1995**, *235*, 484.
(22) Osborn, D. L.; Leahy, D. J.; Neumark, D. *J. Phys. Chem. A* **1997**, *101*, 6583.
(23) Geers, A.; Kappert, J.; Temps, F.; Wiebrecht, J. W. *J. Chem. Phys.* **1994**, *101*, 3618.
(24) Dertinger, S.; Geers, A.; Kappert, J.; Wiebrecht, J.; Temps, F. *Faraday Discuss.* **1996**, *102*, 31.
(25) Chiang, S. Y.; Hsu, Y. C.; Lee, Y. P. *J. Chem. Phys.* **1989**, *90*, 81.
(26) Brossard, S. D.; Carrick, P. G.; Chappell, E. L.; Hulegaard, S. C.; Engelking, P. C. *J. Chem. Phys.* **1986**, *84*, 2459.
(27) Ebata, T.; Yanagishita, H.; Obi, K.; Tanaka, I. *Chem. Phys.* **1982**, *69*, 27.
(28) Leighton, P. *Photochemistry of Air Pollution*; Academic Press: New York, 1961.
(29) Finlayson, B.; Pitts, J. N. Jr. *J. Am. Chem. Soc.* **1974**, *96*, 6554.
(30) Levy, H. I. *Planet. Space Sci.* **1973**, *21*, 575.
(31) Baldwin, A. C.; Barker, J. R.; Golden, D. M.; Hendry, D. G. *J. Am. Phys. Chem.* **1977**, *81*, 2483.
(32) Powers, D. E.; Pushkarsky, M.; Miller, T. A. *Chem. Phys. Letts.* **1995**, *247*, 548.